Electrolyte Additive Enabled Low Temperature Lithium Metal Batteries

Journal:	*Materials Chemistry Frontiers*
Manuscript ID	QM-RES-02-2022-000180.R1
Article Type:	Research Article
Date Submitted by the Author:	09-Apr-2022
Complete List of Authors:	Zhang, Yiwen; Dartmouth College, Thayer School of Engineering Luo, Jianmin; Dartmouth College, Thayer School of Engineering Wang, Chuanlong; Dartmouth College, Thayer School of Engineering Hu, Xiaofei; Dartmouth College, Thayer School of Engineering Matios, Edward; Dartmouth College, Thayer School of Engineering Li, Weiyang; Dartmouth College, Thayer School of Engineering

SCHOLARONE™ Manuscripts

Electrolyte Additive Enabled Low Temperature Lithium Metal Batteries†

Yiwen Zhang, Jianmin Luo, Chuanlong Wang, Xiaofei Hu, Edward Matios and Weiyang Li*

Thayer School of Engineering, Dartmouth College, 14 Engineering Drive, Hanover, NH 03755, USA. E-mail: weiyang.li@dartmouth.edu

†Electronic supplementary information (ESI) available.

Abstract

One of the key challenges in the development of energy storage devices such as batteries is the ability to operate efficiently under cold environments. Here, we demonstrate a dioxolane-based electrolyte with dimethyl sulfoxide (DMSO) as an additive, which helps the nucleation of lithium and the construction of a robust solid electrolyte interphase (SEI) layer on lithium metal electrode at extremely cold condition. Cryogenic transmission electron microscopy and X-ray photoelectron spectroscopy are utilized to thoroughly characterize the microstructure and composition of the SEI. A series of electrochemical tests are conducted at temperatures as low as -80 °C, and the results demonstrate the SEI is resilient to the stripping and plating cycles of lithium metal in cold environments. Moreover, lithium metal batteries with the DMSO added electrolyte can deliver a discharge capacity of 51 mA h g^{-1} at -40 °C under a current rate of 0.2C. This work provides fundamental insights into the development of lithium metal batteries in harsh environments.

Keywords: Lithium metal anodes, electrolyte additive, solid electrolyte interphase, low temperature batteries, cryogenic electron microscopy

Introduction

The growing necessity of lithium-ion batteries (LIBs) as an indispensable energy source for portable electronics, electric vehicles, and grid applications has motivated a plethora of research over the past decades.[1-4] However, the inevitable battery failure at subzero temperatures remains one of the great challenges for the applications of LIB.[5] Specifically, the increased internal resistance and sluggish ion diffusion in cold environments lead to declined charge-delivering capability, which deteriorates both the energy and power output of LIBs.[6] So far, while several approaches have been proposed to improve the low temperature (LT) performance of conventional LIBs, the problem of restricted ion diffusion in graphite anodes is inevitable.[7-9]

The revival of lithium (Li) metal batteries has provided new insights into the development of LT batteries owing to the distinctive Li metal anode design.[10-13] In recent years, multiple attempts have been made to develop a Li metal battery system for LT conditions. For instance, low-viscosity solvents such as liquefied gas, diethyl ether, and ethyl acetate were shown to regulate the nucleation behavior of Li and extend the operational temperature of Li metal batteries to the ultra-low range.[14-16] Meanwhile, building a LiF-rich solid electrolyte interphase (SEI) was proven to be an effective way to achieve a protective Li anode surface and improve the LT battery stability.[17, 18] Although significant efforts have been made, the development of LT Li metal battery system is still in its infancy, and the underlying mechanism for the poor battery performance in cold environments still remains elusive.

The cyclic ether, 1,3-dioxolane (DOL), is well recognized as an essential electrolyte component for Li metal batteries. The low viscosity and melting point of DOL enables fast Li ion diffusion at LT and its potential of forming a uniform SEI stabilizes the Li metal anode during the electrochemical stripping/plating process.[19, 20] In DOL-based electrolytes, a ring-

opening reaction was observed to cause a rapid accumulation of oligoethoxides on Li anode surface and thus forming a flexible polymeric SEI.[21, 22] Despite these attractive properties of DOL, the irreversible electrolyte decomposition and polymerization over the cycling of Li metal can continuously deteriorate the cell efficiency, especially at LT.[23, 24] Thus, the composition of the DOL-based electrolyte needs to be specifically tuned to enable uniform Li nucleation/growth and the formation of a robust SEI on Li metal in cold conditions.

Herein, we develop a DOL-based electrolyte containing dimethyl sulfoxide (DMSO) as an additive, which contributes to substantial improvements in both Li nucleation and SEI formation of Li metal anode at ultra-low temperatures down to -80 °C. Extensive characterization techniques, including cryogenic transmission electron microscopy (Cryo-TEM), scanning electron microscopy (SEM), X-ray photoelectron spectroscopy (XPS), and energy dispersive X-ray spectroscopy (EDX) are conducted to elucidate the surface morphology, microstructure and chemical composition of the Li metal surface and the SEI. Moreover, Li metal batteries with high capacity and stable cycling are achieved at ultra-low temperatures using the DMSO/DOL electrolyte.

Experimental section

Electrolyte preparation

The electrolyte solvents, including DOL (Sigma-Aldrich), 1,2-dimethoxyethane (DME, 99.5%, Sigma-Aldrich) and DMSO (VWR) were dried with molecular sieves (4 Å, Alfa Aesar) before use. Li salts including lithium perchlorate (LiClO$_4$, 99%, Beantown Chemical) and lithium bis(trifluoromethanesulfonimide) (LiTFSI, 99%, Acros Organics) were dried in an argon

(Ar)-filled glovebox (Mbraun) at 120 °C for 4 h before use. The electrolytes were prepared by dissolving the Li salts in the organic solvents in an Ar-filled glovebox.

Cell fabrication

2032-type coin cells were assembled in an Ar-filled glovebox for electrochemical performance tests. In galvanostatic cycling tests, the Li/Li symmetric cells were fabricated with polished Li metal foils (99.9%, Alfa Aesar) cut into 11 mm diameter disks as electrodes, 16 mm diameter Celgard (2400) as separator, and 60 μL of the as-prepared electrolyte.

For Coulombic efficiency (CE) measurements, Li/stainless steel (SS) cells were assembled with SS as the working electrode, Li metal disk as the counter electrode, Celgard separator (2400) and 60 μl of electrolyte. For impedance tests, SS/SS symmetric cells were assembled with SS, Celgard separator (2400) and 60 μl of electrolyte.

For Li metal battery demonstration, lithium iron phosphate (LFP) was used as cathode. The cathode slurry was made by dispersing 80 wt% of LFP (MTI Corporation), 10 wt% of conductive carbon (Super P, 99+%, Alfa Aesar), and 10 wt% of polyvinylidene fluoride (PVDF, Arkema) in the N-methyl-2-pyrrolidone (NMP, 99.5%, Alfa Aesar) solvent. After that, the slurry was spread on aluminum foil using doctor blade and dried at 80 °C under vacuum for 4 h. The as-fabricated LFP cathodes were 11 mm diameter disks with active material loading >2 mg/cm^2. The Li/LFP cells were assembled with LFP cathode, Li disk anode, Celgard separator (2400) and 60 μl of DMSO/DOL electrolyte.

Electrochemical measurement

The electrochemical performance tests of assembled cells were carried out using a Land battery test system (CT2001A, Wuhan LAND Electronics Co., Ltd). The electrochemical impedance spectroscopy (EIS) measurements were performed using an electrochemical

workstation (VMP3, biologic science instruments). The testing temperature ranging from room temperature (RT, 25 °C) to -80 °C was precisely controlled during the cycling. Tests at -20 °C were performed by loading the cells into sealed SS containers immersing in the oil bath (silicone bath fluid, Clearco Products Co, Inc) of a thermostatic circulator (JW-1040, Hebei GuoHui Equipments Co., Ltd). Tests at lower temperatures from -40 to -80 °C and step-wise temperature testing from 0 to -80 °C were operated in the ultra-low temperature chamber (MC-812, ESPEC Corp.). All the cells were stabilized for at least 1 h before testing.

Materials characterization

Laser Raman Spectra (LRS, Horiba labRAM HR Evolution) was collected at a wavelength of 532 nm to investigate the solvation behavior of electrolytes. The samples were tested in a standard quartz cuvette.

SEM (Tescan Vega3) and EDX (PV6300/00 PLE, EDAX Inc.) were employed to investigate the morphology of dendrite growth and chemical composition of the Li anode surface. The samples were prepared by assembling Li/Cu cells with Li metal and Cu electrodes, Celgard separator (2400), and 60 μl of electrolyte. Li metal was electrodeposited on Cu substarte at 0.5 mA cm^{-2} for 8 hours at temperatures from RT to -80 °C before the cells were disassembled in Ar-filled glovebox. The Li deposited Cu substrates were washed with DOL solvent and dried before imaging.

Cryo-TEM was performed to study the micro-structure and chemical composition of the SEI formed on Li dendrite surface. The experiment was conducted with a Tecnai F20ST TEM and a single tilt nitrogen cryo-transfer holder (Gatan model 626). The samples were prepared by assembling Li/Cu cells with Li metal and Cu grid electrodes, Celgard separator (2400), and 60 μl of electrolyte. Li Metal was electrodeposited on Cu grid at 0.25 mA cm^{-1} for 1 hour at RT.

Following that, the cells were disassembled in an Ar-filled glovebox, and the Cu grids were washed with DOL solvent and dried before loading into the Cryo-TEM holder under Ar protection. Liquid nitrogen (LN) was loaded in the Cryo-TEM holder before imaging.

XPS (PHI Versaprobe II scanning XPS microprobe) was conducted with a 0.47 eV system resolution using a monochromatic 1486.7 X-ray source to examine the chemical composition of the SEI. The samples were prepared by assembling Li/Cu cells with Li metal and Cu electrodes, Celgard separator (2400), and 60 ul of electrolyte. After 5 cycles of repeated Li plating and stripping at 0.5 mA cm^{-2} for 2 h at RT, the Li metal was fully stripped from the Cu substrate to a cut off voltage of 1.0 V. The cells were disassembled in Ar-filled glovebox, and the Cu substrates were washed with DOL solvent and dried before testing.

Results and discussion

We first conducted electrochemical tests on various DOL-based electrolytes to identify the optimal electrolyte formulation at -20 °C. As shown in Figure 1a, galvanostatic charge/discharge tests were conducted on the Li/Li symmetric cells with three different DOL-based electrolytes consisting of 1M LiTFSI in a mixture of DOL and DME (50:50 volume ratio), 1M LiTFSI in pure DOL, and 1M LiClO$_4$ in pure DOL, respectively. As a result, the DOL/LiClO$_4$ electrolyte stood out with the lowest and most stable overpotential of less than 0.02 V after 500 hours cycling at 0.5 mA cm^{-2} and 1 mA h cm^{-2}, while the other two candidates showed a much higher overpotential of more than 0.1 V. Additionally, DOL/LiClO$_4$ electrolyte also demonstrated stable cycling in the subsequent rate tests with slight impedance increase, under both high current density (1 to 5 mA cm^{-2} at 1 mA h cm^{-2}) and high capacity (1 to 5 mA h cm^{-2} at 1 mA cm^{-2}) conditions at -20 °C (Figure 1b). One of the critical problems of LT batteries

is the rapidly increasing internal resistance that leads to performance deterioration under LT condition.[25] In this regard, the DOL/LiClO$_4$ electrolyte can potentially be employed for more extreme temperature environments with minimal voltage fluctuation. To further consolidate it, we reduced the testing temperature to -40 °C and illustrated the differences in the cycling performance of DOL/LiClO$_4$ electrolyte under various temperatures (Figure 1c). At both RT and -20 °C, the cells exhibited stable cycling with low overpotential <0.01 V and <0.02V, respectively, at 0.5 mA cm^{-2} and 1 mA h cm^{-2}. Although the overpotential gradually enlarged at -40 °C over the 400 hours of stable cycling, it still stayed within a relatively small range of ~ 0.1 V at 0.5 mA cm^{-2} and 1 mA h cm^{-2}. As the DOL/LiClO$_4$ electrolyte exhibited an outstanding performance among the candidates, it was employed as the primary electrolyte in the following study at lower temperatures.

While the DOL/LiClO$_4$ electrolyte showed stable Li metal plating and stripping behavior in Li/Li symmetric cells, a relatively low CE was observed in the Li/SS cells. The average CE was shown to be about 80% at RT and reduced to 72% and 76% when the temperature was decreased to -20 °C and -40 °C (Figure 2a-d) at 0.5 mA cm^{-2} with a cutoff voltage at 0.5 V. It is reported that a Lewis base could stabilize DOL-based electrolyte and improve the cycling efficiency by neutralizing the Lewis acidity of the electrolyte.[26] Hence, we introduced DMSO, which can function as a Lewis base, as an electrolyte additive into this system to further improve its performance under LT conditions. After optimizing the volume ratio between DOL and DMSO (Figure 2a and Figure S1), it was found that adding 5 vol% of DMSO into the DOL/LiClO$_4$ electrolyte was shown to be effective in improving the CE of Li stripping/plating. We further compared the CE performance of pure DOL electrolyte and DMSO/DOL electrolyte at different temperatures arranging from RT to -40 °C (Figure 2a-d). At RT, the CE in DMSO

added electrolyte was observed to be > 90% for 30 cycles. When tested at -20 °C and -40 °C, the

DMSO added electrolyte also maintained a relatively high CE for ~90% on average after 30

cycles. The bar chart (Figure 2d) summarized the average CEs of these two electrolytes over 30

cycles at different temperatures, showing that the addition of DMSO largely improves the CE of

DOL electrolyte across a wide range of temperatures. Notably, the DMSO/DOL electrolyte went

through a slightly lower CE during the first several cycles, and this process was observed to take

longer time at lower temperatures.

Moreover, the long-term cycling performance in Li/Li symmetric cells at different

temperatures with DMSO/DOL electrolyte was shown in Figure 2e. At RT, the overpotential was

observed to be around 0.05 V at 0.5 mA cm^{-2} and 1 mA h cm^{-2}. When the temperature was

decreased to -20 °C and -40 °C, the symmetric cells exhibited higher voltage at around 0.1 V and

0.15 V, respectively, and the overpotential increased gradually during the 400 hours cycling.

Although the addition of DMSO slightly increased the overpotential compared to pure DOL

electrolyte, it effectively stabilized the stripping and plating of Li metal and improved the overall

cell performance. The performance of DMSO/DOL electrolyte was further evaluated at low

temperatures below -40 °C. In this case, we adopted a step-wise temperature testing scheme

(Figure 2f and Figure S2), and conducted galvanostatic cycling tests with Li/Li symmetric cells

in DOL electrolyte and DMSO/DOL electrolyte at a series of temperatures that decreased

continuously from 0 °C to -80 °C at 0.25 mA cm^{-2} and 0.5 mA h cm^{-2}. Between 0 °C and -40 °C,

the overpotential of DMSO/DOL symmetric cell was observed to successively increase so as in

pure DOL electrolyte. When temperature was further reduced to -60 °C and -80 °C, the cell with

DMSO/DOL electrolyte cycled for more than 60 hours with a relatively low overpotential less

than 0.2V, while the batteries with pure DOL electrolyte failed immediately under the same condition.

To better understand the cycling behavior of these electrolytes at low temperatures, we investigated the Li deposition at different temperatures using SEM. Figure 3 and Figure S3 showed the morphology of Li metal plated on Cu substrate from RT to -80 °C. It is noted that the size of the Li deposit was observed to gradually decrease with decreasing temperatures for both electrolytes, consistent with the prior literature.[24] For instance, the size of plated Li that was formed at RT with DOL electrolyte was found to be around 5 to 10 μm in diameter. When deposited at -20 °C and -40 °C, the size reduced to 2 to 3 μm and 0.5 to 1 μm in diameter, respectively. Similar trend was observed from RT to -40 °C in DMSO/DOL electrolytes. Interestingly, the Li deposition behavior started to differ significantly when the temperature dropped to -60 °C and -80 °C. In DOL electrolyte, Li metal was scarcely deposited on the Cu substrate at -60 °C (Figure 3e), leaving a spotty pattern; at -80 °C, hardly any Li can be observed, resulting in an almost bare Cu substrate (Figure 3g). In comparison, in the DMSO/DOL electrolyte, Li metal can still go through nucleation and growth process, exhibiting a relatively uniform Li metal layer with smaller particle size (around 0.5 μm in diameter at -60 °C and 0.2 μm in diameter at -80 °C). This phenomenon is in good agreement with the step-wise temperature test results, in which the cell with pure DOL electrolyte experienced rapid failure at temperatures lower than -40 °C, while the one with DMSO/DOL electrolyte established relatively stable cycling performance down to -80 °C.

We find that the addition of DMSO can improve both the conductivity and the salt solubility of the DOL-based electrolyte, especially at low temperatures. At 0 °C and -40 °C (Figure S4), the DMSO additive largely increased the electrolyte conductivity by 3 times. At -

80 °C, DMSO additive further secured a complete Li salt solvation and relatively low impedance in the electrolyte, while the precipitation of $LiClO_4$ salt was observed in DOL electrolyte, which resulted in an abrupt concentration reduction of $LiClO_4$ salt. Since the ionic conductivity of liquid electrolyte is strongly dependent on salt concentration, a large increase of the impedance was observed in DOL electrolyte at -80 °C.[27] Moreover, DMSO possesses both high Gutmann donor number (DN) and acceptor number (AN) and thus displays a high affinity to both anions and cations in the electrolyte in a strong solvation form, while DOL has relatively low DN and AN, indicating a weaker interaction with the ions.[28] Therefore, when DMSO was added into the primary DOL electrolyte, Li ions would prefer to coordinate with DMSO molecules to form $Li[DMSO]_4$ clusters.[29] This change in the solvation structure can be revealed by Raman spectroscopy (Figure S5). For pure DMSO, the characteristic C-S symmetric stretching peak and asymmetric stretching peak could be found at 670 cm^{-1} and 698 cm^{-1}, respectively. While, for DMSO/DOL electrolyte, both peaks went through a 9 cm^{-1} blue shift, representing the breakage of the self-associations between DMSO molecules and the coordination of Li-ion with DMSO.[29-31] The formation of $Li[DMSO]_4$ clusters could turn DMSO into the dominant component in the solvation sheath of Li ions, thus resulting in preferentially interaction with the electrode surface and determining both the Li deposition behavior and the SEI formation.[32]

The SEI formation behavior induced by DMSO additive could be further validated by a stabilization process observed in electrochemical tests. For instance, the DMSO/DOL electrolyte exhibited slightly lower CE during the first several cycles from RT to -40 °C. These stabilization cycles could be attributed to the initial formation of a protective SEI film and its temperature dependent behavior indicated that temperature could be one of the key factors of SEI formation in DMSO/DOL electrolyte. Similar stabilization phenomenon was observed in the symmetric

cells as well. The symmetric cells using DMSO/DOL electrolyte underwent certain voltage fluctuations during the first several cycles (Figure S6), while the cells using DOL electrolyte showed a stable curve.

The microstructure and composition of the SEI was investigated by Cryo-TEM and XPS. As shown in Figure 4a-f, for both pure DOL and DMSO/DOL electrolytes, a thin SEI layer composed of amorphous matrix and evenly distributed nano-crystallites was found on the surface of Li metal deposited at 0.25 mA cm^{-2} and 0.25 mAh cm^{-2} at RT. In the SEI formed in pure DOL electrolyte, a large amount of Li_2O crystallites was identified by the presence of (111) Li_2O lattice fringe and the diffraction rings in the selective area electron diffraction (SAED). A similar structure was found in the SEI formed with DMSO/DOL electrolyte, but fewer Li_2O crystallites and a larger amorphous region was observed, as illustrated in the colored graphs. Also, LiOH crystallite was also identified in the SEI, which could be due to the trace amount of H_2O in the DMSO solvent.[33, 34] Comparing the thickness of these two SEI films, the thickness slightly increased from ~10 nm in DOL electrolyte to ~15 nm in DMSO/DOL electrolyte, which is consistent with the relatively higher overpotential observed in the symmetric cell testing of DMSO/DOL electrolyte.

Figure 4g-l showed the C1s, O1s, and S2p XPS spectra of the SEI formed in pure DOL and DMSO/DOL electrolyte, respectively. The SEI was obtained after 5 cycles of Li plating/stripping at 0.5 mA cm^{-2} and 1 mAh cm^{-2} at RT. The C1s peak that represents the aliphatic carbons (C-C) at 284.6 eV was used as the reference for calibration. Two peaks at 285.7 eV and 289.6 eV in the C1s spectra were observed and could be assigned to the CH_2-CH_2-O and O-CH_2-O functional group, respectively, which may be ascribed to the major decomposition products from the DOL ring-opening reaction with two different cleavage sites.[22, 35, 36] These two

linkage structures could be further confirmed in the O1s spectra by the two peaks at 531.6 eV and 532.8 eV. Noteworthy, it was found that DMSO largely altered the chemical composition of the amorphous region by participating in the SEI formation, resulting in a slightly higher intensity of CH_2-CH_2-O peaks and, specifically, a higher content of S species.[37] As shown in the S2p spectra, three peaks at 161.0 eV, 163.4 eV, and 166.5 eV were identified, convincing the presence of Li_2S, C-S-C, and O=S=O, respectively, in the amorphous region of the SEI.[29, 38, 39]

EDX was further performed to reveal the elemental analysis of the SEI composition. As shown in Figure S7, after 5 cycles of Li plating/stripping at 0.5 mA cm^{-2} and 1 mAh cm^{-2}, the weight percentage of Cl in the SEI was observed to be 9.9 wt% in pure DOL electrolyte and 7.7 wt% in DMSO/DOL electrolyte at RT. In both cases, the Cl percentage gradually decreased with decreasing temperature. The Cl content in the SEI, presented as ClO_4^- and LiCl (Figure S8), was attributed to the $LiClO_4$ salt,[40, 41] and was largely influenced by the working temperature. Note that the Cl percentage of the SEI formed in DMSO/DOL electrolyte was observed to be lower than that in pure DOL electrolyte at the same temperature, which indicates that the addition of DMSO may help to prevent Li salt decomposition and precipitation. Meanwhile, the S content in the SEI of DMSO/DOL electrolyte was observed to be stable throughout the wide temperature range, which only slightly fluctuated between 7 wt% and 10 wt%, showing a high level of composition consistency against temperature change.

According to the above-mentioned experimental observations, we propose that the superior performance of the DMSO/DOL electrolyte at low operating temperatures could be due to the reason that DMSO molecules would dominate the solvation sheath of Li-ion in the DMSO/DOL electrolyte, thus impacting the Li deposition behavior and the SEI formation process (Figure S9). On one hand, it facilitates the nucleation of Li metal and enables stable Li

stripping/plating in a wide temperature range from RT to -80 °C. On the other hand, it helps to construct a SEI with high stability and composition consistency over temperature change. Specifically, DOL could induce the formation of a SEI composed of Li_2O crystallites and amorphous organic matrix, and the addition of DMSO further reduces the crystallinity of the SEI and introduces S-containing species into the amorphous region.

Pairing with LFP as cathode (theoretical capacity: 170 mA h g^{-1}), Li metal batteries were assembled using the DMSO/DOL electrolyte and tested under various cold environments. The cathode is composed of 80 wt% LFP, 10 wt% conductive carbon, and 10 wt% PVDF. The active material loading is > 2 mg cm^{-2} and the current rate is 0.2 C. The cells were tested under the step-wise temperature condition, running continuously from 0 °C down to -80 °C (Figure 5a and 5b). The typical charge/discharge profiles of the batteries with DMSO/DOL electrolyte were shown in Figure 5a. It can deliver a discharge capacity of 107 mA h g^{-1} at 0 °C, 95 mA h g^{-1} at -10 °C, 82 mA h g^{-1} at -20 °C, and 51 mA h g^{-1} at -40 °C, showing a good capacity retention at LT. Noteworthy, the specific capacity could still be maintained at 47 mA h g^{-1} after 6 stable cycles of charge/discharge at -40 °C before the temperature goes down to -60 °C. Even when the temperature was reduced to -60 °C, the battery could still deliver a discharge capacity for around 20 mA h g^{-1}. Long-term cycling tests were further conducted (Figure 5c) at -20 °C and -40 °C. When the cell was directly operated at -20 °C and 0.2 C (without the step-wise temperature process), the specific capacity slightly increased over cycling, showing a steady energy output and reached a capacity of 77 mA h g^{-1} after 50 cycles. When operated at -40 °C, the cell showed a specific capacity of 40 mA h g^{-1} after 50 cycles of charge/discharge. It is noted that, when operated at the same temperature, the capacities of the cells in the long-term cycling tests (e.g. 40 mA h g^{-1} at -40 °C) were slightly lower than those tested under the step-wise temperature

condition (e.g. 51 mA h g^{-1} at -40 °C). Thus, an activation process at relatively higher temperatures, such as the charge/discharge at 0 °C in the step-wise temperature condition, might be beneficial to the following cycling at lower temperatures by helping the formation of the SEI and the activation of the LFP cathode. Figure 5d displayed the typical charge/discharge profiles of the long-term cycling at -20 °C and -40 °C. Longer charging curves were observed for the first charging process at both temperatures due to the formation of SEI, consistent with the symmetric cell testing. The cells exhibited stable charge and discharge curves over 50 cycles with distinctive plateaus. Thus, the DMSO/DOL electrolyte was proved to be compatible with commercial cathode material, especially at various LT conditions, and could potentially be employed for further practical applications.

Conclusions

In summary, we developed a novel electrolyte for Li metal anodes by introducing DMSO as an additive in the DOL-based electrolyte, which enables stable stripping/plating behavior in cold environments down to -80 °C. It was found that the addition of DMSO into the electrolyte largely impacted both Li nucleation process and the microstructure and chemical composition of the SEI film formed on the Li anode surface at LT conditions. This work has provided a facile and efficient approach for the further development of batteries at crucial environments for defense, space, and terrestrial applications.

Conflicts of Interest

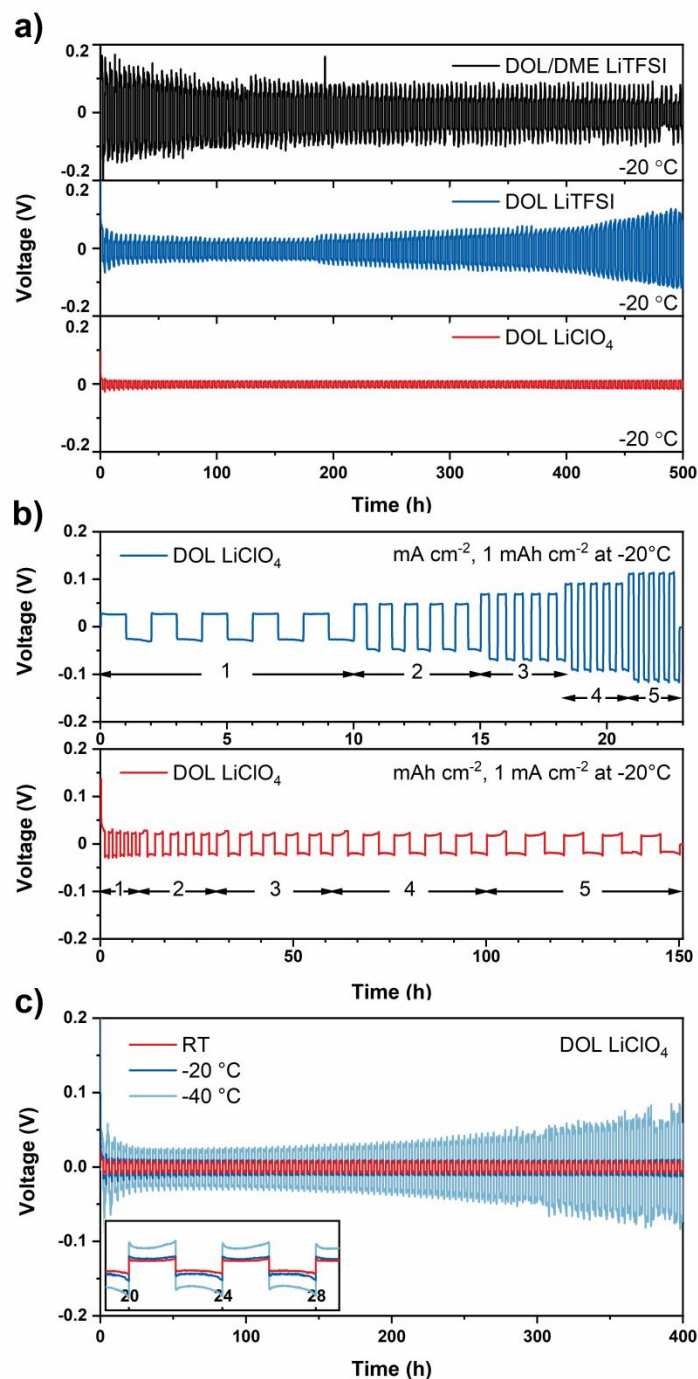There are no conflicts to declare.

Acknowledgements

Figure 1. Galvanostatic cycling performance and rate performance of DOL-based electrolytes at LT. a) Long-term cycling of 1M LiTFSI in DOL/DME, 1M LiTFSI in DOL, and 1M LiClO$_4$ in DOL at 0.5 mA cm^{-2} and 1 mA h cm^{-2} at -20 °C. b) Rate performance of 1M LiClO$_4$ in DOL electrolyte at various current density (1 to 5 mA cm^{-2} at 1 mA h cm^{-2}) and various capacity (1 to 5 mA h cm^{-2} at 1 mA cm^{-2}) at -20 °C. c) Long-term cycling of 1M LiClO$_4$ in DOL at RT, -20 °C, and -40 °C at 0.5 mA cm^{-2} and 1 mA h cm^{-2}. Inset: enlarged voltage profile of the 5th and the 6th cycles.
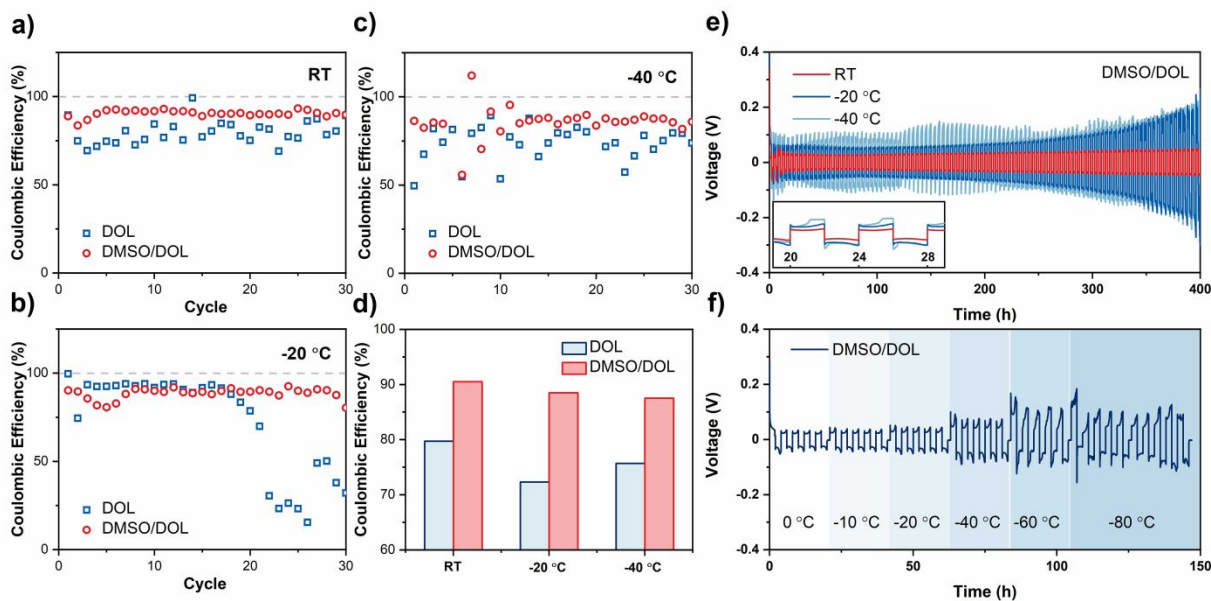
Figure 2. The electrochemical performance improvement induced by DMSO additive. Comparing the CEs of DOL and DMSO/DOL electrolyte at a) RT; b) -20 °C; c) -40 °C, and d) the average CE over 30 cycles at 0.5 mA cm^{-2} and 1 mA h cm^{-2} with a cutoff voltage at 0.5 V. e) Long-term cycling of DMSO/DOL electrolyte in Li/Li symmetric cells at RT, -20 °C, and -40 °C at 0.5 mA cm^{-2} and 1 mA h cm^{-2}. The inset showed enlarged details in the 5th and the 6th cycle. f) Step-wise symmetric cycling tests for DMSO/DOL electrolyte under varying temperatures from 0 °C to -80 °C at 0.25 mA cm^{-2} and 0.5 mA h cm^{-2}.
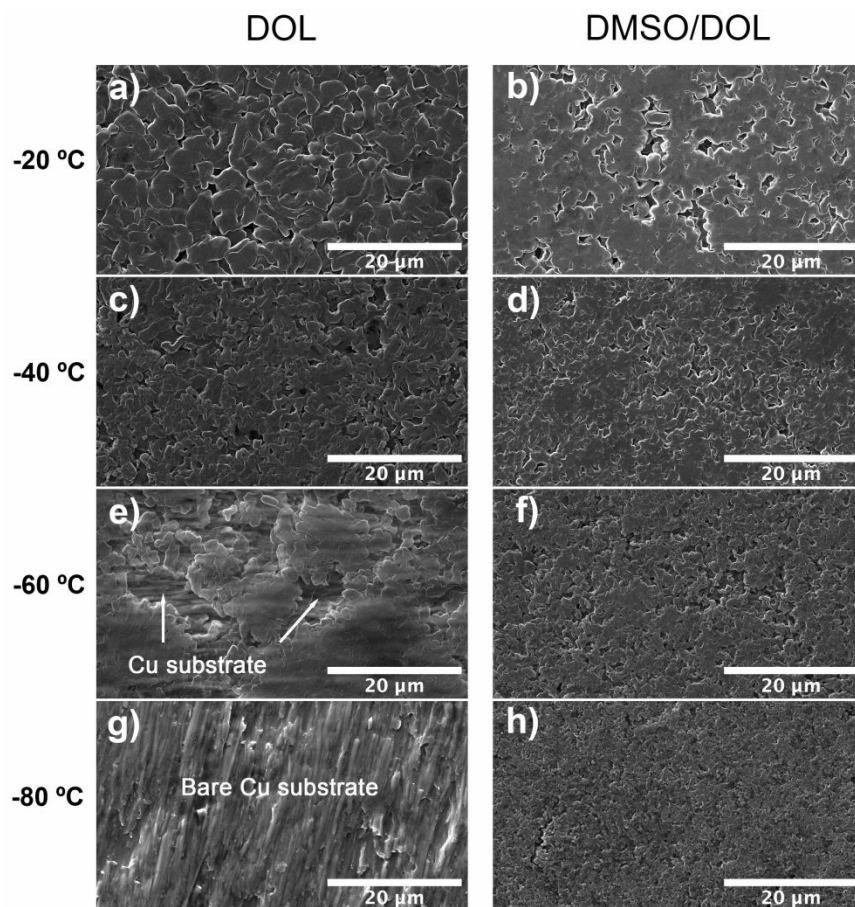
Figure 3. The morphology of Li deposited on Cu substrate at 0.5 mA cm^{-2} for 8 hours with pure DOL electrolyte and DMSO/DOL electrolyte, respectively. The samples in a) and b) were prepared at -20 °C, c) and d) at -40 °C, e) and f) at -60 °C, g) and h) at -80 °C.
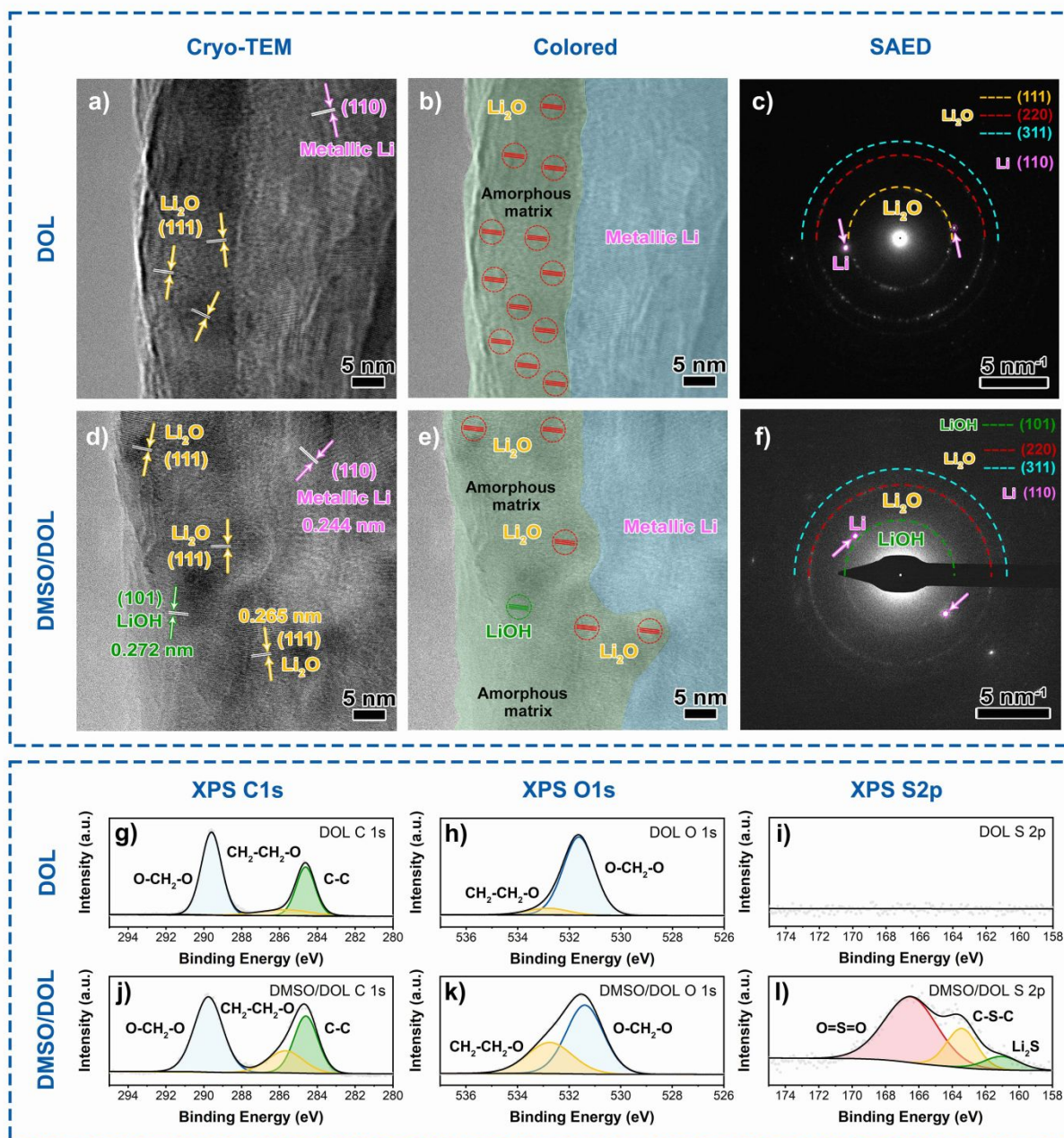
Figure 4. Cryo-TEM and XPS characterization of the SEI formed on Li metal anode. Cryo-TEM graphs of SEI formed in a) DOL electrolyte and d) DMSO/DOL electrolyte, respectively. b) and e) are colored Cryo-TEM graphs. The SEI was marked in green and the Li metal was marked in blue. The red circles represented the distribution of Li_2O crystallites and the green circles represented the LiOH crystallites in the SEI layer. The SAED patterns of the SEI formed in DOL electrolyte and DMSO/DOL electrolyte were shown in c) and f), respectively. High resolution XPS spectra for the SEI formed in DOL electrolyte and DMSO/DOL electrolyte were displayed, respectively, with C1s spectra in g) and j), O1s spectra in h) and k), S2p spectra in i) and l).
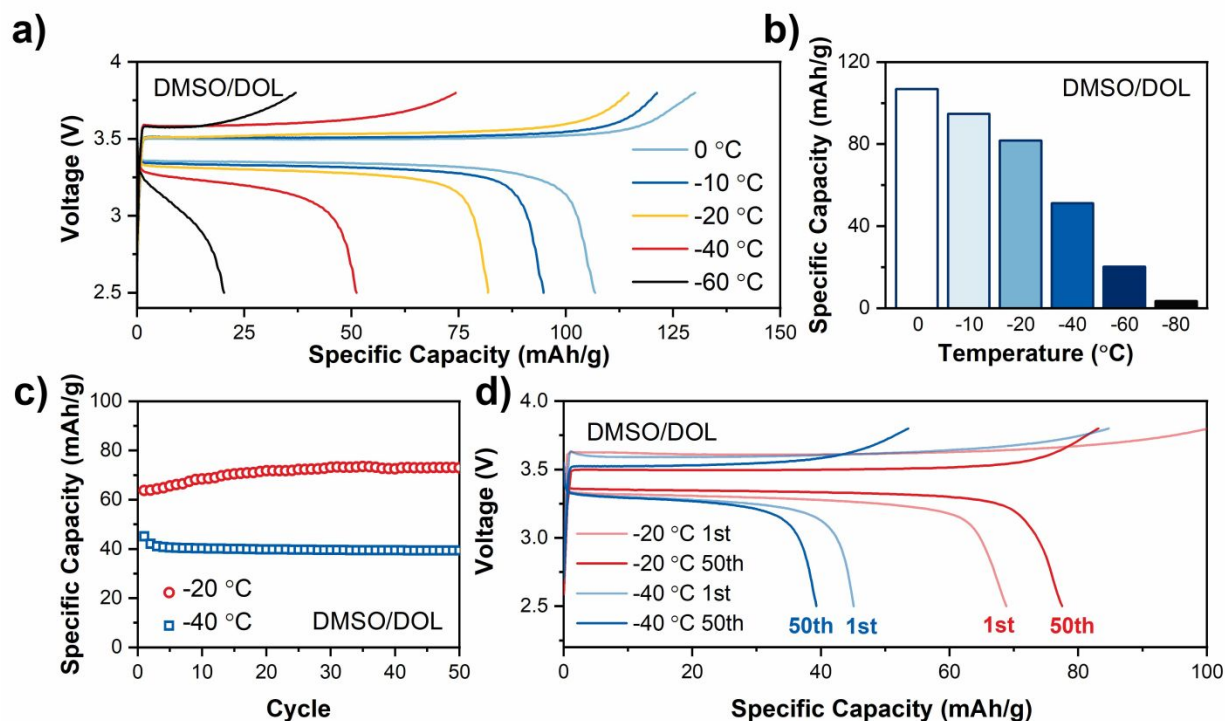
Figure 5. The LFP/Li cell performance demonstration using DMSO/DOL electrolyte at 0.2 C and at different low temperatures. a) Step-wise charge/discharge profiles from 0 °C to -60 °C. b) Bar-plot of the specific capacities in the step-wise cycling. c) Long-term cycling performance at -20 °C and -40 °C (without the temperature step-wise process). d) The charge/discharge profiles of the 1st and 50th cycles at -20 °C and -40 °C.

References

1. J.-M. Tarascon and M. Armand, Issues and challenges facing rechargeable lithium batteries, *Nature*, 2001, **414**, 359-367.
2. Z. P. Cano, D. Banham, S. Ye, A. Hintennach, J. Lu, M. Fowler and Z. Chen, Batteries and fuel cells for emerging electric vehicle markets, *Nature Energy*, 2018, **3**, 279-289.
3. A. W. Schäfer, S. R. H. Barrett, K. Doyme, L. M. Dray, A. R. Gnadt, R. Self, A. O'Sullivan, A. P. Synodinos and A. J. Torija, Technological, economic and environmental prospects of all-electric aircraft, *Nature Energy*, 2018, **4**, 160-166.
4. B. Dunn, H. Kamath and J.-M. Tarascon, Electrical energy storage for the grid: a battery of choices, *Science*, 2011, **334**, 928-935.
5. C. Y. Wang, G. Zhang, S. Ge, T. Xu, Y. Ji, X. G. Yang and Y. Leng, Lithium-ion battery structure that self-heats at low temperatures, *Nature*, 2016, **529**, 515-518.
6. Y. Ji, Y. Zhang and C.-Y. Wang, Li-Ion Cell Operation at Low Temperatures, *Journal of The Electrochemical Society*, 2013, **160**, A636-A649.
7. M. C. Smart, B. V. Ratnakumar and S. Surampudi, Use of Organic Esters as Cosolvents in Electrolytes for Lithium-Ion Batteries with Improved Low Temperature Performance, *Journal of The Electrochemical Society*, 2002, **149**.
8. M. C. Smart, B. V. Ratnakumar, L. D. Whitcanack, K. B. Chin, S. Surampudi, H. Croft, D. Tice and R. Staniewicz, Improved low-temperature performance of lithium-ion cells with quaternary carbonate-based electrolytes, *Journal of Power Sources*, 2003, **119-121**, 349-358.
9. M. C. Smart, B. V. Ratnakumar, K. B. Chin and L. D. Whitcanack, Lithium-Ion Electrolytes Containing Ester Cosolvents for Improved Low Temperature Performance, *Journal of The Electrochemical Society*, 2010, **157**.
10. D. Lin, Y. Liu and Y. Cui, Reviving the lithium metal anode for high-energy batteries, *Nat Nanotechnol*, 2017, **12**, 194-206.
11. B. Liu, J.-G. Zhang and W. Xu, Advancing Lithium Metal Batteries, *Joule*, 2018, **2**, 833-845.
12. J. Liu, Z. Bao, Y. Cui, E. J. Dufek, J. B. Goodenough, P. Khalifah, Q. Li, B. Y. Liaw, P. Liu, A. Manthiram, Y. S. Meng, V. R. Subramanian, M. F. Toney, V. V. Viswanathan, M. S. Whittingham, J. Xiao, W. Xu, J. Yang, X.-Q. Yang and J.-G. Zhang, Pathways for practical high-energy long-cycling lithium metal batteries, *Nature Energy*, 2019, **4**, 180-186.
13. Z. Li, H. Zhang, X. Sun and Y. Yang, Mitigating Interfacial Instability in Polymer Electrolyte-Based Solid-State Lithium Metal Batteries with 4 V Cathodes, *ACS Energy Letters*, 2020, **5**, 3244-3253.
14. C. S. Rustomji, Y. Yang, T. K. Kim, J. Mac, Y. J. Kim, E. Caldwell, H. Chung and Y. S. Meng, Liquefied gas electrolytes for electrochemical energy storage devices, *Science*, 2017, **356**.
15. J. Holoubek, H. Liu, Z. Wu, Y. Yin, X. Xing, G. Cai, S. Yu, H. Zhou, T. A. Pascal, Z. Chen and P. Liu, Tailoring Electrolyte Solvation for Li Metal Batteries Cycled at Ultra-Low Temperature, *Nat Energy*, 2021, **2021**.
16. X. Dong, Y. Lin, P. Li, Y. Ma, J. Huang, D. Bin, Y. Wang, Y. Qi and Y. Xia, High-Energy Rechargeable Metallic Lithium Battery at -70 degrees C Enabled by a Cosolvent Electrolyte, *Angew Chem Int Ed Engl*, 2019, **58**, 5623-5627.

17.   Y. Gao, T. Rojas, K. Wang, S. Liu, D. Wang, T. Chen, H. Wang, A. T. Ngo and D. Wang, Low-temperature and high-rate-charging lithium metal batteries enabled by an electrochemically active monolayer-regulated interface, *Nature Energy*, 2020, **5**, 534-542.

18.   A. C. Thenuwara, P. P. Shetty, N. Kondekar, S. E. Sandoval, K. Cavallaro, R. May, C.-T. Yang, L. E. Marbella, Y. Qi and M. T. McDowell, Efficient Low-Temperature Cycling of Lithium Metal Anodes by Tailoring the Solid-Electrolyte Interphase, *ACS Energy Letters*, 2020, **5**, 2411-2420.

19.   J. Xu, X. Wang, N. Yuan, J. Ding, S. Qin, J. M. Razal, X. Wang, S. Ge and Y. Gogotsi, Extending the low temperature operational limit of Li-ion battery to −80 °C, *Energy Storage Materials*, 2019, **23**, 383-389.

20.   Q. Zhao, X. Liu, J. Zheng, Y. Deng, A. Warren, Q. Zhang and L. Archer, Designing electrolytes with polymerlike glass-forming properties and fast ion transport at low temperatures, *Proc Natl Acad Sci U S A*, 2020, **117**, 26053-26060.

21.   D. Aurbach, O. Youngman and P. Dan, The electrochemical behavior of 1, 3-dioxolane—LiClO4 solutions—II. Contaminated solutions, *Electrochimica acta*, 1990, **35**, 639-655.

22.   Q. Liu, A. Cresce, M. Schroeder, K. Xu, D. Mu, B. Wu, L. Shi and F. Wu, Insight on lithium metal anode interphasial chemistry: Reduction mechanism of cyclic ether solvent and SEI film formation, *Energy Storage Materials*, 2019, **17**, 366-373.

23.   M. Alamgir, R. Moulton and K. Abraham, Li+-conductive polymer electrolytes derived from poly (1, 3-dioxolane) and polytetrahydrofuran, *Electrochimica acta*, 1991, **36**, 773-782.

24.   A. C. Thenuwara, P. P. Shetty and M. T. McDowell, Distinct Nanoscale Interphases and Morphology of Lithium Metal Electrodes Operating at Low Temperatures, *Nano Lett*, 2019, **19**, 8664-8672.

25.   J. Jaguemont, L. Boulon and Y. Dubé, A comprehensive review of lithium-ion batteries used in hybrid and electric vehicles at cold temperatures, *Applied Energy*, 2016, **164**, 99-114.

26.   Y. Gofer, M. Ben-Zion and D. Aurbach, Solutions of LiAsF6 in 1, 3-dioxolane for secondary lithium batteries, *Journal of power sources*, 1992, **39**, 163-178.

27.   L. O. Valøen and J. N. Reimers, Transport Properties of LiPF6-Based Li-Ion Battery Electrolytes, *Journal of The Electrochemical Society*, 2005, **152**.

28.   L. Lutz, D. Alves Dalla Corte, M. Tang, E. Salager, M. Deschamps, A. Grimaud, L. Johnson, P. G. Bruce and J.-M. Tarascon, Role of Electrolyte Anions in the Na–O2 Battery: Implications for NaO2 Solvation and the Stability of the Sodium Solid Electrolyte Interphase in Glyme Ethers, *Chemistry of Materials*, 2017, **29**, 6066-6075.

29.   N. Togasaki, T. Momma and T. Osaka, Enhanced cycling performance of a Li metal anode in a dimethylsulfoxide-based electrolyte using highly concentrated lithium salt for a lithium–oxygen battery, *Journal of Power Sources*, 2016, **307**, 98-104.

30.   Z. Wang, B. Huang, S. Wang, R. Xue, X. Huang and L. Chen, Vibrational spectroscopic study of the interaction between lithium perchlorate and dimethylsulfoxide, *Electrochimica acta*, 1997, **42**, 2611-2617.

31.   X. Xuan, J. Wang, Y. Zhao and J. Zhu, Experimental and computational studies on the solvation of lithium tetrafluorobrate in dimethyl sulfoxide, *Journal of Raman Spectroscopy*, 2007, **38**, 865-872.

32.   Y. Zhang, Y. Zhong, Z. Wu, B. Wang, S. Liang and H. Wang, Solvent Molecule Cooperation Enhancing Lithium Metal Battery Performance at Both Electrodes, *Angew Chem Int Ed Engl*, 2020, **59**, 7797-7802.

33.   Y. Hui and R. D. Webster, Absorption of water into organic solvents used for electrochemistry under conventional operating conditions, *Anal Chem*, 2011, **83**, 976-981.

34.   Y. J. Jang, T.-T. H. Nguyen, H. Park, S. A. Chae, S. A. Cho, Y. H. Jang, S. An, O. H. Han, K. Kang, D. Oh, S. J. Kang, H.-C. Kim and D. H. Kim, Investigation of Li–O2 Battery Performance Integrated with RuO2 Inverse Opal Cathodes in DMSO, *ACS Applied Energy Materials*, 2019, **2**, 5109-5115.

35.   N. Kim, Y. Myung, H. Kang, J. W. Lee and M. Yang, Effects of Methyl Acetate as a Co-Solvent in Carbonate-Based Electrolytes for Improved Lithium Metal Batteries, *ACS Appl Mater Interfaces*, 2019, **11**, 33844-33849.

36.   T. Jin, Y. Wang, Z. Hui, B. Qie, A. Li, D. Paley, B. Xu, X. Wang, A. Chitu, H. Zhai, T. Gong and Y. Yang, Nonflammable, Low-Cost, and Fluorine-Free Solvent for Liquid Electrolyte of Rechargeable Lithium Metal Batteries, *ACS Appl Mater Interfaces*, 2019, **11**, 17333-17340.

37.   G. Bieker, M. Winter and P. Bieker, Electrochemical in situ investigations of SEI and dendrite formation on the lithium metal anode, *Phys Chem Chem Phys*, 2015, **17**, 8670-8679.

38.   H. Ota, T. Akai, H. Namita, S. Yamaguchi and M. Nomura, XAFS and TOF–SIMS analysis of SEI layers on electrodes, *Journal of Power Sources*, 2003, **119-121**, 567-571.

39.   Q. Zhao, X. Liu, S. Stalin, K. Khan and L. A. Archer, Solid-state polymer electrolytes with in-built fast interfacial transport for secondary lithium batteries, *Nature Energy*, 2019, **4**, 365-373.

40.   K. Kanamura, H. Takezawa, S. Shiraishi and Z. i. Takehara, Chemical reaction of lithium surface during immersion in LiClO4 or LiPF6/DEC electrolyte, *Journal of the Electrochemical Society*, 1997, **144**, 1900.

41.   X. Liang, Q. Pang, I. R. Kochetkov, M. S. Sempere, H. Huang, X. Sun and L. F. Nazar, A facile surface chemistry route to a stabilized lithium metal anode, *Nature Energy*, 2017, **2**.